Available online at www.sciencedirect.com
SCIENCE DIRECT®
Journal of Computational Physics 203 (2005) 287–304
JOURNAL OF COMPUTATIONAL PHYSICS
www.elsevier.com/locate/jcp

On mass conservation in least-squares methods

P. Bolton *, R.W. Thatcher

Department of Mathematics, UMIST, Sackville Street, P.O. Box 88, Manchester M60 1QD, UK

Received 7 November 2003; received in revised form 19 August 2004; accepted 19 August 2004
Available online 21 September 2004

Abstract

We compare three least-squares finite element reformulations of the Stokes equations, paying particular attention to mass conservation. The first problem we approximate has a simple analytical solution over a convex region. Even for this simple problem, without special treatment of the conservation of mass term, very poor numerical solutions may result. Sufficiently weighting this term leads to a dramatic improvement in the results over a range of test problems.

Keywords: First-order; Least-squares; Finite elements; Conservation of mass; Stokes flows; Stress and stream functions

1. The least-squares finite element method

In recent years there has been considerable interest in the least-squares finite element method as a way of obtaining solutions of systems of partial differential equations; see for instance [8,25]. This technique seems promising as the linear systems which arise are positive-definite and symmetric and hence amenable to fast direct or iterative solution methods.

For the system of N_{eq} partial differential equations

$$Lu = f \quad \text{in } \Omega$$

with boundary conditions

$$Bu = g \quad \text{on } \Gamma, \tag{1}$$

an L^2 least-squares functional

* Corresponding author.
E-mail address: paul.j.bolton@student.umist.ac.uk (P. Bolton).

0021-9991/$ - see front matter
doi:10.1016/j.jcp.2004.08.013

$$\|Lu - f\|_0^2 = \sum_{i=1}^{N_{\text{eq}}} \|L_i u - f_i\|_0^2 \tag{2}$$

is defined. We let $u = (u_1,u_2,\ldots,u_m)^{\mathrm{T}} \in U$ and $v = (v_1,v_2,\ldots,v_m)^{\mathrm{T}} \in V$ where functions in U satisfy the boundary conditions (1) and the functions in V satisfy the homogeneous form of these conditions. The function $u \in U$ such that the least-squares functional (2) is minimised satisfies the equation

$$\int_\Omega \sum_{i=1}^{N_{\text{eq}}} (L_i u - f_i) L_i v \, \mathrm{d}\Omega = 0 \quad \forall v \in V.$$

Usually the differential operator is first-order requiring at most H^1 regularity in U and V. Higher order equations are reformulated as a first-order system; see [16,26,29]. Examples in fluid dynamics of systems recast in this way are the Stokes and Navier–Stokes equations for incompressible flow [4], the convection–diffusion equations [22] and the Stokes equations for compressible flow [14]. However, (2) is provably optimal only for elliptic systems of Petrovsky type; see [33].

It has been observed in solutions of a first-order reformulation of the Stokes equations that mass conservation is not generally well enforced; see [18,20]. Particular attention was paid in these references to the loss of mass in solutions in a multiply connected domain. Here, we consider solutions of a number of different first-order reformulations of the Stokes equations. We show that even in a convex region the loss of mass in a numerical solution obtained using the least-squares method can be disastrous.

2. The Stokes equations for incompressible flow in the plane

For fluid of velocity $\vec{u} = (u_1, u_2)$ and at pressure p the Stokes equations for incompressible, steady flow can be expressed as

$$-\nu\nabla^2\vec{u} + \nabla p = \vec{f}, \tag{3}$$

$$\nabla \cdot \vec{u} = 0. \tag{4}$$

The parameter ν is the viscosity. The enclosed flow conditions for this problem are

$$\vec{u} = g_b(x,y) \quad \text{on } \Gamma, \tag{5}$$

$$\int_\Omega p \, \mathrm{d}\Omega = 0. \tag{6}$$

2.1. The stress and stream function reformulation

In [31], a first-order system of equations is derived which is equivalent to (3) and (4) at $\vec{f} = 0$. This system is in terms of the stream and stress functions. The stream function ψ is defined so that

$$u_1 = \psi_y, \tag{7}$$

$$u_2 = -\psi_x. \tag{8}$$

The stresses can be represented by a 2×2 symmetric tensor

$$\sigma = \begin{pmatrix} \sigma_{11} & \sigma_{12} \\ \sigma_{21} & \sigma_{22} \end{pmatrix}.$$

For fluids in steady flow and in the absence of body forces the divergence of the stress tensor is zero

$$\nabla \cdot \sigma = 0. \tag{9}$$

Postulating the existence of a sufficiently differentiable stress function ϕ and setting

$$\sigma = \begin{pmatrix} \phi_{yy} & -\phi_{xy} \\ -\phi_{xy} & \phi_{xx} \end{pmatrix} \tag{10}$$

ensures that (9) is true.

For incompressible fluids

$$\sigma = -pI + 2\nu d,$$

where I is the identity matrix and d is the deformation tensor

$$d = \frac{1}{2}\begin{pmatrix} 2\dfrac{\partial u_1}{\partial x} & \dfrac{\partial u_1}{\partial y} + \dfrac{\partial u_2}{\partial x} \\ \dfrac{\partial u_1}{\partial y} + \dfrac{\partial u_2}{\partial x} & 2\dfrac{\partial u_2}{\partial y} \end{pmatrix}.$$

So using the variables defined in (7), (8) and (10) we have

$$\begin{aligned} \phi_{yy} &= -p + 2\nu\psi_{xy}, \\ \phi_{xx} &= -p - 2\nu\psi_{xy}, \\ -\phi_{xy} &= -\nu\psi_{xx} + \nu\psi_{yy}. \end{aligned}$$

Eliminating p we have

$$-\phi_{xx} + \phi_{yy} = 4\nu\psi_{xy}, \tag{11}$$

$$-\phi_{xy} = -\nu\psi_{xx} + \nu\psi_{yy}. \tag{12}$$

By introducing the variables

$$U_1 = \phi_x, \quad U_2 = \phi_y, \quad U_3 = \psi_x, \quad U_4 = \psi_y$$

we are able to write (11) and (12) as a first-order system

$$-\frac{\partial U_1}{\partial x} + \frac{\partial U_2}{\partial y} - 2\nu\frac{\partial U_3}{\partial y} - 2\nu\frac{\partial U_4}{\partial x} = f_1, \tag{13}$$

$$\frac{\partial U_1}{\partial y} + \frac{\partial U_2}{\partial x} - 2\nu\frac{\partial U_3}{\partial x} + 2\nu\frac{\partial U_4}{\partial y} = f_2, \tag{14}$$

$$\frac{\partial U_1}{\partial y} - \frac{\partial U_2}{\partial x} = f_3, \tag{15}$$

$$2\nu\frac{\partial U_3}{\partial y} - 2\nu\frac{\partial U_4}{\partial x} = f_4, \tag{16}$$

see [31]. For the Stokes system without body forces the terms f_1–f_4 are all zero. To obtain a least-squares solution we minimise the functional

$$S = \left\| -\frac{\partial U_1}{\partial x} + \frac{\partial U_2}{\partial y} - 2\nu\frac{\partial U_3}{\partial y} - 2\nu\frac{\partial U_4}{\partial x} - f_1 \right\|_0^2 + \left\| \frac{\partial U_1}{\partial y} + \frac{\partial U_2}{\partial x} - 2\nu\frac{\partial U_3}{\partial x} + 2\nu\frac{\partial U_4}{\partial y} - f_2 \right\|_0^2 + \left\| \frac{\partial U_1}{\partial y} - \frac{\partial U_2}{\partial x} - f_3 \right\|_0^2 + \left\| 2\nu\frac{\partial U_3}{\partial y} - 2\nu\frac{\partial U_4}{\partial x} - f_4 \right\|_0^2. \tag{17}$$

We shall henceforth refer to the system of Eqs. (13)–(16) as the S formulation of the Stokes system and shall call (17) the S functional.

Four different forms of boundary condition for the system (13)–(16) are considered in [31]. These are

$$U_1 = g_1(x,y), \quad U_2 = g_2(x,y) \quad \text{on } \Gamma, \tag{18}$$

$$U_3 = g_1(x,y), \quad U_4 = g_2(x,y) \quad \text{on } \Gamma, \tag{19}$$

$$(U_1, U_2)\cdot\hat{n} = g_1(x,y), \quad (U_3, U_4)\cdot\hat{s} = g_2(x,y) \quad \text{on } \Gamma, \tag{20}$$

$$(U_1, U_2)\cdot\hat{s} = g_1(x,y), \quad (U_3, U_4)\cdot\hat{n} = g_2(x,y) \quad \text{on } \Gamma. \tag{21}$$

Further pointwise constraints $\Lambda_i(U)$, $i = 1,\ldots,N_c$ may also be required on the solution when the conditions (18) or (19) are applied; see [31]. The boundary conditions (18) specify the stresses on the boundary whilst (19) correspond to the enclosed flow conditions (5) and (6) on the second-order system (3) and (4). The boundary conditions (20) give the normal velocities and tangential stresses whilst (21) give tangential velocities and normal stresses. The system (13)–(16) with any of these boundary conditions (18)–(21) is shown in [31] to be of Petrovsky type [33] in regions with smooth boundaries. Hence, for $U \in [H^1(\Omega) \cap H^{l+1}(\Omega)]^4$, $l = -1, 0$ the inequality

$$\|U\|_{l+1,\Omega} \leqslant C\left(\|LU\|_{l,\Omega} + \|BU\|_{l+\frac{1}{2},\Gamma} + \sum_{i=1}^{N_c} |\Lambda_i(U)| \right),$$

holds and with homogeneous boundary conditions S is equivalent to a norm on H^1

$$\frac{1}{C}\|U\|_1^2 \leqslant S \leqslant C\|U\|_1^2.$$

Hence it can be shown that approximations on regions with smooth boundaries using linear elements converge at order h in an H^1 metric; see [31,32].

2.2. The velocity–vorticity–pressure reformulation

Another first-order recasting of the Stokes equations is the velocity–vorticity–pressure formulation; see [17,27]. This is probably the formulation most frequently used in work appearing in published studies of least-squares methods; see for example [1,5,7,13,18,20,21,25,28,34].

In deriving this system we utilise the identity

$$-\nabla^2\vec{u} = \nabla\times\nabla\times\vec{u} = \nabla\times\omega,$$

where ω is the vorticity and $\vec{u} = (u_1, u_2)$. This identity holds if $\nabla.\vec{u} = 0$. The system (3) and (4) can then be written as

$$\nu\nabla\times\omega + \nabla p = \vec{f}, \tag{22}$$

$$\omega - \nabla\times\vec{u} = 0, \tag{23}$$

$$\nabla \cdot \vec{u} = 0. \tag{24}$$

We shall use the symbol J to denote this system and the corresponding L^2 least-squares functional

$$J = \|v\nabla \times \omega + \nabla p - \vec{f}\|_0^2 + v^2\|\omega - \nabla \times \vec{u}\|_0^2 + v^2\|\nabla \cdot \vec{u}\|_0^2, \tag{25}$$

see [13,19,20]. In our experiments we have enforced the enclosed flow conditions (5) and (6). But the system (22)–(24) with enclosed flow conditions is not elliptic in the sense of Petrovsky and hence the least-squares functional (25), which is simply an L^2 functional of the form (2), is not fully H^1 coercive. Hence we expect convergence of only order h in L^2. However, it has been established theoretically that when the conditions (5) and (6) are enforced the functional

$$J_1 = \|v\nabla \times \omega + \nabla p - \vec{f}\|_0^2 + v^2\|\omega - \nabla \times \vec{u}\|_1^2 + v^2\|\nabla \cdot \vec{u}\|_1^2 \tag{26}$$

is coercive in $[H^2(\Omega)]^2 \times H^1(\Omega) \times H^1(\Omega)$; see [7,8,20]. We let $s > 0$ and define the spaces

$$H_0^s(\Omega) = \{v \in H^s(\Omega) : v = 0 \quad \text{on } \Gamma\},$$

$$L_0^2(\Omega) = \left\{v \in L^2(\Omega) : \int_\Omega v \, d\Omega = 0\right\},$$

$$\tilde{H}^s(\Omega) = H^s(\Omega) \cap L_0^2(\Omega).$$

Furthermore, we let $\vec{u} \in [H_0^2(\Omega)]^2$, $p \in \tilde{H}^1(\Omega)$ and $\omega \in H^1(\Omega)$. Then it can be shown that

$$\frac{1}{C}\left(\|\vec{u}\|_2^2 + \|p\|_1^2 + \|\omega\|_1^2\right) \leqslant J_1(\vec{u}, p, \omega),$$

see [8]. Also

$$J_1(\vec{u}, p, \omega) \leqslant C\left(\|\vec{u}\|_2^2 + \|p\|_1^2 + \|\omega\|_1^2\right).$$

So the solutions of (26) satisfy the relation

$$\|\vec{u}\|_2 + \|p\|_1 + \|\omega\|_1 \leqslant C\|\vec{f}\|_0,$$

see [7].

2.3. The velocity–velocity gradient–pressure reformulation

A third planar formulation is the velocity–velocity gradient–pressure formulation, as proposed in [12]; see also [29]. A very similar reformulation has been used in the application of least-squares methods to the solution of the linear elasticity equations, which are related to the Stokes equations; see [12], in which both are considered as special cases of the system

$$-v\nabla^2\vec{u} + \nabla p = \vec{f}, \tag{27}$$

$$\nabla \cdot \vec{u} + \delta p = g. \tag{28}$$

The parameter δ is zero for the Stokes equations. A new variable U is introduced

$$U = \nabla\vec{u}^{\mathrm{T}} = \begin{pmatrix} \dfrac{\partial u_1}{\partial x} & \dfrac{\partial u_1}{\partial y} \\ \dfrac{\partial u_2}{\partial x} & \dfrac{\partial u_2}{\partial y} \end{pmatrix}. \tag{29}$$

Eqs. (27) and (28) can be written in the form

$$-v(\nabla \cdot U)^{\mathrm{T}} + \nabla p = \vec{f},$$

$$\nabla \cdot \vec{u} + \delta p = g,$$

$$U - \nabla\vec{u}^{\mathrm{T}} = 0.$$

In [12] this form of the system is designated as G_1. This system with conditions (5) and (6) is not fully H^1 coercive and an L^2 least-squares functional of the form (2) is inappropriate. The G_1 least-squares functional is

$$G_1(U,\vec{u},p) = \| - \nu(\nabla\cdot U)^{\mathrm{T}} + \nabla p - \vec{f}\|_{-1}^2 + \nu^2\|\nabla\cdot\vec{u} + \delta p - g\|_0^2 + \nu^2\|U - \nabla\vec{u}^{\mathrm{T}}\|_0^2. \tag{30}$$

The supplementary equations

$$\nabla\times U = 0,$$
$$\nabla(\text{trace } U + \delta p - g) = 0$$

lead to the least-squares functional G_2

$$\begin{aligned} G_2(U,\vec{u},p) = {} & \| - \nu(\nabla\cdot U)^{\mathrm{T}} + \nabla p - \vec{f}\|_0^2 + \nu^2\|\nabla\cdot\vec{u} + \delta p - g\|_0^2 + \nu^2\|U - \nabla\vec{u}^{\mathrm{T}}\|_0^2 \\ & + \nu^2\|\nabla\times U\|_0^2 + \nu^2\|\nabla(\text{trace } U + \delta p - g)\|_0^2. \end{aligned} \tag{31}$$

We note that trace $U = \nabla\cdot\vec{u}$. In solving this functional the conditions (5) and (6) must be supplemented with the boundary conditions

$$U\times\hat{n} = G_b(x,y). \tag{32}$$

We let D be the distance to the nearest vertex of Ω. Then the further equation

$$D^{-1}(\text{trace } U - g) = 0,$$

taken together with the equations of G_2 for the Stokes case gives the system from which is generated the least-squares functional which is designated G_3 in [12]. The solution of the G_3 formulation is found by looking for the values of U, $\vec{u}$ and p which minimise the functional

$$\begin{aligned} G_3(U,\vec{u},p) = {} & \| - \nu(\nabla\cdot U)^{\mathrm{T}} + \nabla p - \vec{f}\|_0^2 + \nu^2\|\nabla\cdot\vec{u} - g\|_0^2 + \nu^2\|U - \nabla\vec{u}^{\mathrm{T}}\|_0^2 + \nu^2\|\nabla\times U\|_0^2 \\ & + \nu^2\|\nabla(\text{trace } U - g)\|_0^2 + \nu^2\|D^{-1}(\text{trace } U - g)\|_0^2. \end{aligned} \tag{33}$$

The appropriate conditions are again (5), (6) and (32). We shall refer to these conditions as the enclosed flow conditions for the G_3 formulation.

In [12] coercivity and continuity bounds on the functionals (30), (31) and (33) are obtained for the case in which $\vec{f} = 0$ and $g = 0$. Following [12] we define the spaces

$$U_0 = \left(V\in H^1(\Omega)^{n^2} : \hat{n}\times V = \vec{0} \quad \text{on } \Gamma\right),$$
$$U_1 = \left(V\in U_0 : \delta \text{ trace } V \in L^2(\Omega)\right),$$
$$V_1 = L^2(\Omega)^{n^2}\times H_0^1(\Omega)^n \times L_0^2(\Omega),$$
$$V_2 = U_0\times H_0^1(\Omega)^n \times \left(H^1(\Omega)\setminus\Re\right),$$
$$V_3 = U_1\times H_0^1(\Omega)^n \times \left(H^1(\Omega)\setminus\Re\right).$$

For the planar case the appropriate spaces are given by setting $n = 2$. The G_1 functional (30) has the bounds

$$\frac{1}{C}\left(\nu^2\|U\|_0^2 + \nu^2\|\vec{u}\|_1^2 + \|p\|_0^2\right) \leqslant G_1(U,\vec{u},p) \quad \forall (U,\vec{u},p)\in V_1$$

and

$$G_1(U,\vec{u},p) \leqslant C\left(\nu^2\|U\|_0^2 + \nu^2\|\vec{u}\|_1^2 + \|p\|_0^2\right) \quad \forall (U,\vec{u},p)\in V_1.$$

These hold provided the approximation to the velocity is at least quadratic. The G_2 functional (31) satisfies the bounds

$$\frac{1}{C}\left(\nu^2\|U\|_1^2+\nu^2\|\vec{u}\|_1^2+\|p\|_1^2\right)\leqslant G_2(U,\vec{u},p)\quad\forall(U,\vec{u},p)\in V_2$$

and

$$G_2(U,\vec{u},p)\leqslant C\left(\nu^2\|U\|_1^2+\nu^2\|\vec{u}\|_1^2+\|p\|_1^2\right)\quad\forall(U,\vec{u},p)\in V_2.$$

These bounds on $G_2(U,\vec{u},p)$ hold if the boundary of the region has continuity $C^{1,1}$. The bounds on the G_3 functional (33) are

$$\frac{1}{C}\left(\nu^2\|U\|_1^2+\nu^2\|D^{-1}\text{ trace }U\|_0^2+\nu^2\|\vec{u}\|_1^2+\|p\|_1^2\right)\leqslant G_3(U,\vec{u},p)\quad\forall(U,\vec{u},p)\in V_3 \tag{34}$$

and

$$G_3(U,\vec{u},p)\leqslant C\left(\nu^2\|U\|_1^2+\nu^2\|D^{-1}\text{ trace }U\|_0^2+\nu^2\|\vec{u}\|_1^2+\|p\|_1^2\right)\quad\forall(U,\vec{u},p)\in V_3. \tag{35}$$

The relations (34) and (35) are valid in convex polygons; see [12].

Another reformulation in which the gradients of the velocity also appear as variables is presented in [15], where it is referred to as the acceleration–pressure formulation.

2.4. Equation weighting

An extension of the least-squares method for systems of equations allows for different weights in the functional (2); see [2]. The functional (2) generalises to

$$\sum_{i=1}^{N_{\text{eq}}}W_i\|L_iu-f_i\|_0^2,\quad W_i>0.$$

This has a minimum when

$$\int_\Omega\sum_{i=1}^{N_{\text{eq}}}W_iL_iuL_iv\,\mathrm{d}\Omega=\int_\Omega\sum_{i=1}^{N_{\text{eq}}}W_if_iL_iv\,\mathrm{d}\Omega,$$

where v is an element of a test space V, with elements of the same order of continuity as the trial solutions and which are homogeneous on the boundary Γ of Ω.

With the aim of more strongly enforcing mass conservation for solutions satisfying enclosed flow conditions, we weight the appropriate terms in the various functionals. So the weighted J functional J_W is

$$J_W=\|\nu\nabla\times\omega+\nabla p-\vec{f}\|_0^2+\nu^2\|\omega-\nabla\times\vec{u}\|_0^2+W\nu^2\|\nabla\cdot\vec{u}\|_0^2, \tag{36}$$

whilst the weighted G_3 functional $G_{3,W}$ is

$$\begin{aligned}G_{3,W}=&\|-\nu(\nabla\cdot U)^{\mathrm{T}}+\nabla p-\vec{f}\|_0^2+W\nu^2\|\nabla\cdot\vec{u}-g\|_0^2+\nu^2\|U-\nabla\vec{u}^{\mathrm{T}}\|_0^2+\nu^2\|\nabla\times U\|_0^2\\&+\nu^2\|\nabla(\text{trace }U-g)\|_0^2+\nu^2\|D^{-1}(\text{trace }U-g)\|_0^2.\end{aligned}$$

In dealing with the S functional, we follow [31,32] in weighting not only the residual of the mass-conservation equation (16) but also the residual of (15) by the same amount, so that the weighted S functional takes the form

$$S_W = \left\| -\frac{\partial U_1}{\partial x} + \frac{\partial U_2}{\partial y} - 2v\frac{\partial U_3}{\partial y} - 2v\frac{\partial U_4}{\partial x} - f_1 \right\|_0^2 + \left\| \frac{\partial U_1}{\partial y} + \frac{\partial U_2}{\partial x} - 2v\frac{\partial U_3}{\partial x} + 2v\frac{\partial U_4}{\partial y} - f_2 \right\|_0^2 + W\left\| \frac{\partial U_1}{\partial y} - \frac{\partial U_2}{\partial x} - f_3 \right\|_0^2 + W\left\| 2v\frac{\partial U_3}{\partial y} - 2v\frac{\partial U_4}{\partial x} - f_4 \right\|_0^2. \quad (37)$$

In our experience W must be reasonably large to have a substantial effect on the quality of the solution. However, for a very large value of W the resulting linear system becomes ill-conditioned. In the experiments presented here we have chosen $W = 10^3$ but optimisation of this parameter may be possible.

3. Poiseuille flow in a long channel

We have obtained approximate solutions of the S, J and G_3 formulations and the corresponding weighted formulations for Poiseuille flow in the region $[0,20]\times[0,1]$. In the S formulation the analytical solution is

$$U_1 = v\left(x^2 + y^2 - 2Lx - y\right),$$
$$U_2 = v(2xy - 2Ly + L - x),$$
$$U_3 = 0,$$
$$U_4 = y(1-y).$$

The analytical solutions in the variables of the J and G formulations can also be written down in simple forms. Throughout our calculations we set $v = 1$.

The elements we use are triangular and the interpolation is linear. A typical 8×4 grid is illustrated in Fig. 1.

3.1. Solutions of the S formulation

For these results enclosed flow conditions (19) are enforced. We also set $U_1 = 0$ and $U_2 = 20$ at $(0,0)$ and $U_2 = 0$ at $(20,1)$. In Tables 1 and 2 we show the total flow across the lines $x = \{0,5,10,15,20\}$.

Table 1 shows that when using the S formulation a very large quantity of mass is lost in the middle of the channel, even on highly refined grids. For example, in the solution on the 1280×64 over 20% of the flow is lost in the middle of the region. Convergence in the velocity is quite slow between the grids; see the first two

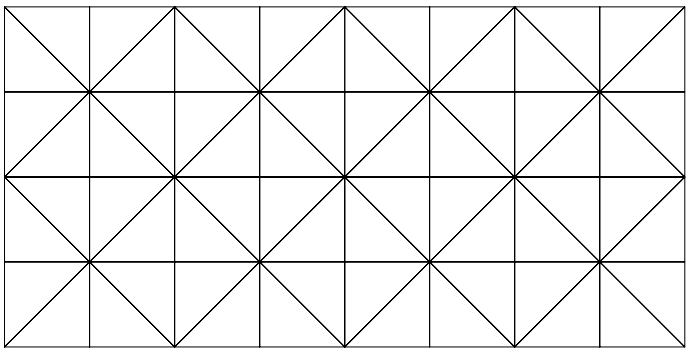

Fig. 1. Union Jack grid of size 8×4.

columns of results in Table 3. Even between highly refined grids the rate of convergence is much less than the optimal order h^2 in L^2. With weighting, that is the S_W formulation, much less flow is lost on all grids. The flow in the middle of the channel is about 99.95% of the inflow in the solution on the 1280×64 grid; see Table 2. We see from Table 3 that even between the coarsest grids the rate of convergence in the velocity is approximately order h in H^1 which is in accord with the theoretical asymptotic rates. Moreover, we observe convergence of order h^2 in L^2.

3.2. Solutions of the J formulation

Using the J formulation and minimising the L^2 functional (25) we get a very similar set of results to those obtained with the S formulation. Table 4 shows that there is a large amount of mass lost in the solution of the J formulation although slightly less than in the solution of the S formulation on a given grid; compare Table 4 with Table 1. The velocities converge somewhat faster; compare Table 6 with Table 3.

As before there is almost no mass lost in the solution obtained by minimising the J_W functional, especially on the more refined grids; see Table 5. We observe that the velocities converge at a rate of order h in H^1 and order h^2 in L^2; see Table 6. The rate of convergence in L^2 is faster than the provable rate for solutions of the velocity–vorticity–pressure system satisfying enclosed flow conditions: in this case with linear elements we expect convergence only of order h in L^2.

3.3. Solutions of the G_3 formulation

These results are obtained by enforcing the enclosed flow conditions (5), (6) and (32) for Poiseuille flow. We see that a large quantity of flow is lost in the solutions obtained by minimising the G_3 functional (33); see Table 7. The rate of convergence of the velocity in H^1 between the finest grids on which we have obtained solutions, the 320×16 and 640×32 grids, seems to be order h; see Table 9. The rate of convergence in L^2 between these grids is slightly greater than order h. These solutions are more accurate than those obtained by minimising the S functional (17) or the J functional (25). In assessing the relative merits of each solution process, attention must be paid to the fact that there are more variables at each node in the G_3 formulation and overall more equations in the system.

Only a small proportion of the mass is lost between the inlet and the centre of the channel in the solution of the $G_{3,W}$ formulation; see Table 8. Table 9 shows that the approximations to the velocities in the solution of the $G_{3,W}$ functional are considerably more accurate than those in the solution of the unweighted functional. They converge at a rate of order h in H^1 and order h^2 in L^2.

Table 1
Axial flow in the solution of the S formulation

$n_x \times n_y$	Axial flow				
	$x = 0$	$x = 5$	$x = 10$	$x = 15$	$x = 20$
80×4	0.15625	0.00121	0.00002	0.00121	0.15625
160×8	0.16406	0.01034	0.00130	0.01034	0.16406
320×16	0.16602	0.04153	0.01870	0.04153	0.16602
640×32	0.16650	0.09433	0.07403	0.09433	0.16650
1280×64	0.16663	0.13931	0.13061	0.13931	0.16663

Table 2
Axial flow in the solution of the S_W formulation

$n_x \times n_y$	Axial flow				
	$x = 0$	$x = 5$	$x = 10$	$x = 15$	$x = 20$
80×4	0.15625	0.14505	0.14140	0.14505	0.15625
160×8	0.16406	0.16074	0.15963	0.16074	0.16406
320×16	0.16602	0.16515	0.16486	0.16515	0.16602
640×32	0.16650	0.16628	0.16621	0.16628	0.16650
1280×64	0.16663	0.16657	0.16655	0.16657	0.16663

Table 3
Errors in the solutions of the S and S_W formulations

$n_x \times n_y$	Errors in the solution of the S formulation		Errors in the solution of the S_W formulation	
	$\|\vec{u} - \vec{u}_h\|_{0,2}$	$\| \vec{u} - \vec{u}_h\|_{1,2}$	$\|\vec{u} - \vec{u}_h\|_{0,2}$	$\| \vec{u} - \vec{u}_h\|_{1,2}$
80×4	0.75294	2.38364	0.10060	0.66861
160×8	0.69802	2.21483	0.02739	0.32644
320×16	0.57080	1.80954	0.00700	0.16176
640×32	0.33930	1.07584	0.00176	0.08068
1280×64	0.12981	0.41230	0.00044	0.04031

Table 4
Axial flow in the solution of the J formulation

$n_x \times n_y$	Axial flow				
	$x = 0$	$x = 5$	$x = 10$	$x = 15$	$x = 20$
160×8	0.16406	0.04355	0.02112	0.04355	0.16406
320×16	0.16602	0.07930	0.05645	0.07930	0.16602
640×32	0.16650	0.12472	0.11172	0.12472	0.16650
1280×64	0.16663	0.15295	0.14847	0.15295	0.16663

Table 5
Axial flow in the solution of the J_W formulation

$n_x \times n_y$	Axial flow				
	$x = 0$	$x = 5$	$x = 10$	$x = 15$	$x = 20$
160×8	0.16406	0.16290	0.16252	0.16290	0.16406
320×16	0.16602	0.16572	0.16563	0.16572	0.16602
640×32	0.16650	0.16643	0.16641	0.16643	0.16650
1280×64	0.16663	0.16661	0.16660	0.16661	0.16663

3.4. Solutions of the S formulation with outflow conditions

In obtaining a solution of the S formulation we may also apply the boundary conditions

$$U_3 = 0,\ U_4 = y(1-y) \quad \text{on the line } x = 0,$$
$$U_3 = 0,\ U_4 = 0 \quad \text{on the line } y = 0,$$
$$U_3 = 0,\ U_4 = 0 \quad \text{on the line } y = 1,$$
$$U_2 = 0,\ U_3 = 0 \quad \text{on the line } x = 20.$$

Table 6
Errors in the solutions of the J and J_W formulations

$n_x \times n_y$	Errors in the solution of the J formulation		Errors in the solution of the J_W formulation	
	$\|\vec{u} - \vec{u}_h\|_{0,2}$	$\|\vec{u} - \vec{u}_h\|_{1,2}$	$\|\vec{u} - \vec{u}_h\|_{0,2}$	$\|\vec{u} - \vec{u}_h\|_{1,2}$
160×8	0.56251	1.78766	0.01810	0.32314
320×16	0.40715	1.29284	0.00453	0.16138
640×32	0.19843	0.63131	0.00113	0.08067
1280×64	0.06523	0.20947	0.00028	0.04033

Table 7
Axial flow in the solution of the G_3 formulation

$n_x \times n_y$	Axial flow				
	$x = 0$	$x = 5$	$x = 10$	$x = 15$	$x = 20$
80×4	0.15625	0.02770	0.00735	0.02770	0.15625
160×8	0.16406	0.04915	0.02060	0.04915	0.16406
320×16	0.16602	0.08917	0.06145	0.08917	0.16602
640×32	0.16650	0.13278	0.11845	0.13278	0.16650

Table 8
Axial flow in the solution of the $G_{3,W}$ formulation

$n_x \times n_y$	Axial flow				
	$x = 0$	$x = 5$	$x = 10$	$x = 15$	$x = 20$
80×4	0.15625	0.15192	0.15047	0.15192	0.15625
160×8	0.16406	0.16291	0.16253	0.16291	0.16406
320×16	0.16602	0.16573	0.16563	0.16573	0.16602
640×32	0.16650	0.16643	0.16641	0.16643	0.16650

Table 9
Errors in the solutions of the G_3 and $G_{3,W}$ formulations

$n_x \times n_y$	Errors in the solution of the G_3 formulation		Errors in the solution of the $G_{3,W}$ formulation	
	$\|\vec{u} - \vec{u}_h\|_{0,2}$	$\|\vec{u} - \vec{u}_h\|_{1,2}$	$\|\vec{u} - \vec{u}_h\|_{0,2}$	$\|\vec{u} - \vec{u}_h\|_{1,2}$
80×4	0.62277	1.99036	0.07128	0.64894
160×8	0.53993	1.71754	0.01807	0.32313
320×16	0.36993	1.17598	0.00453	0.16138
640×32	0.16553	0.52809	0.00113	0.08067

The fourth condition represents outflow or downstream stress conditions. It is also necessary to have one further pointwise constraint for a unique solution; we choose to fix $U_1 = 0$ at $(0,0)$. With these conditions the loss of mass is even more severe. For instance in the solution of the S formulation on the 1280×64 grid the flow through the line $x = 10$ is only 56.6% of the inflow, whilst the flow through the outlet $x = 20$ is only 44.4% of the inflow. Again, using the weighted functional S_W these poor results can be corrected. In this case about 99.9% of the inflow passes through the line $x = 10$ and 99.8% through the outlet; see [10].

3.5. A note on the grid configuration

We are indebted to one of our reviewers for querying our use of the Union Jack grid, illustrated in Fig. 1, which is known to have special properties not necessarily possessed by other configurations; see for instance [9,30]. Results for the S_W functional on grids composed of unidirectional triangles are much poorer, although results for the unweighted functionals and for the J_W and $G_{3,W}$ functionals are not very different on either form of grid. We have not fully investigated this variation in solutions of the S_W formulation. We note however that recomputing the results in [32] for biharmonic problems without weighting the form of the grid was again not important, whereas with weighting a unidirectional grid gave much poorer results. It seems likely that for a large value of the weight W the grid decomposition property discussed in [3,23,24] becomes important. Thus it seems in solving the Stokes problem, when weighting seems essential, to be clearly advisable to use the Union Jack grid or, in non-rectangular domains, grids which are topologically equivalent; see [10].

3.6. Conditioning

Although the preceding results clearly show that weighting of certain terms can greatly improve the accuracy of least-squares solutions the concern arises that this could increase significantly the condition number of the linear systems. Table 10 gives estimated condition numbers for the linear systems arising from the S and S_W functionals (17) and (37) with the enclosed flow conditions (19) and those arising from the J and J_W functionals (25) and (36) satisfying the conditions (5) and (6). The condition numbers are indeed considerably greater after weighting. However we see that the condition numbers of the weighted systems increase at approximately order h^{-2} whereas the condition numbers of the unweighted systems shown here increase faster than order h^{-2}. Furthermore the rate of increase in the condition numbers of the unweighted functionals falls as the grid is refined and we may speculate that for finer grids than those shown here the condition numbers for unweighted and weighted systems may be close together. We have also obtained the condition numbers for the linear systems arising from the solution of the channel flow problem by use of the G_3 and $G_{3,W}$ functionals. The J system for a given grid is better conditioned than the G_3 system, which in turn is better conditioned than the S system. The condition numbers of the J_W and $G_{3,W}$ systems for a given grid are similar and much smaller than the condition numbers for the S_W system.

4. Higher order elements

We have used the S, J and G_1 formulations and their weighted counterparts on a range of other test problems including flow over a backward facing step, flow past a semicircular restriction and flow around

Table 10
Estimated condition numbers

Grid	Condition numbers			
	S	S_W	J	J_W
80×4	2.90×10^8	2.09×10^{10}	6.42×10^6	4.55×10^8
160×8	2.96×10^9	8.23×10^{10}	7.43×10^7	1.74×10^9
320×16	2.83×10^{10}	3.31×10^{11}	7.84×10^8	7.28×10^9
640×32	2.11×10^{11}	1.36×10^{12}	5.85×10^9	3.41×10^{10}
1280×64	1.16×10^{12}	5.65×10^{12}	3.02×10^{10}	1.80×10^{11}

a cylinder; see [10,11]. Just as with channel flow, using linear elements these functionals give poor results but quite reasonable and encouraging results when weighting is employed. All these test problems are in non-convex regions and the velocities are not in H^2; as expected, the G_2 and G_3 results are very poor.

Few of the least-squares results published elsewhere have been obtained with such low order elements. Hence the loss of mass we have seen in our solutions has not been observed to the same degree. It is important to note that the J and G_1 functionals are not H^1 equivalent and, as a result, the convergence theory has only been developed for quadratic and higher order elements. We note that for the particular case of Poiseuille flow the analytical solution is captured exactly with quadratic elements. However, we have also observed severe loss of mass in solutions of the more complicated test problems even when quadratic or biquadratic elements have been used.

4.1. Mesh-dependent weighting

From the inverse inequality

$$\|V\|_1 \leqslant Ch^{-1}\|V\|_0 \tag{38}$$

we can replace the functional (26) by one which incorporates mesh-dependent weights, namely

$$J_h = \|v\nabla \times \omega + \nabla p - \vec{f}\|_0^2 + v^2h^{-2}\|\omega - \nabla \times \vec{u}\|_0^2 + v^2h^{-2}\|\nabla \cdot \vec{u}\|_0^2, \tag{39}$$

see [2,7,8,20]. This can be solved with H^1 elements. In minimising (39) approximations to the velocity $\vec{u}$ using quadratic or biquadratic elements converge at order h^2 in H^1. If the pressure p and vorticity ω are approximated using either linear or quadratic elements they converge at order h in H^1 and order h^2 in L^2; see [7]. So if the pressure and vorticity are approximated using quadratic or biquadratic elements convergence rates in these variables are suboptimal.

We can also weight the mass conservation term in (39) with an additional factor to give

$$J_{h,W} = \|v\nabla \times \omega + \nabla p - \vec{f}\|_0^2 + v^2h^{-2}\|\omega - \nabla \times \vec{u}\|_0^2 + Wv^2h^{-2}\|\nabla \cdot \vec{u}\|_0^2, \tag{40}$$

see [20]. Generalising (38) a mesh-dependent functional arising from the G_1 system for incompressible flow is

$$G_{1,h} = h^2\| - v(\nabla \cdot U)^{\mathrm{T}} + \nabla p - \vec{f}\|_0^2 + v^2\|\nabla \cdot \vec{u}\|_0^2 + v^2\|U - \nabla\vec{u}^{\mathrm{T}}\|_0^2, \tag{41}$$

and a corresponding weighted functional is

$$G_{1,h,W} = h^2\| - v(\nabla \cdot U)^{\mathrm{T}} + \nabla p - \vec{f}\|_0^2 + Wv^2\|\nabla \cdot \vec{u}\|_0^2 + v^2\|U - \nabla\vec{u}^{\mathrm{T}}\|_0^2, \tag{42}$$

see [8].

4.2. Backward facing step

Here, we present results for a backward facing step. The physical region is illustrated in Fig. 2. We place the re-entrant corner at the origin so that our region is $[-2,0]\times[-1,0]\cup[0,6]\times[-1,1]$. We have approximated the solution of the S and S_W functionals (17) and (37) and the above mesh-dependent functionals (39)–(42) with biquadratic elements for all variables; we believe that being able to use the same elements for all variables is one of the advantages of least-squares methods, even if approximations may then sometimes be suboptimal in some variables. Our elements are square and of uniform size and h is the length of the diagonal. We define a parameter n_y such that the number of nodes on the inflow line $x = -2$ is $n_y + 1$ so that the total number of nodes in the region is $2n_y \times (n_y + 1) + (6n_y + 1) \times (2n_y + 1)$. The grid at $n_y = 4$ is shown in Fig. 3. In Tables 11–14 we show the axial flow through successive portions of the region.

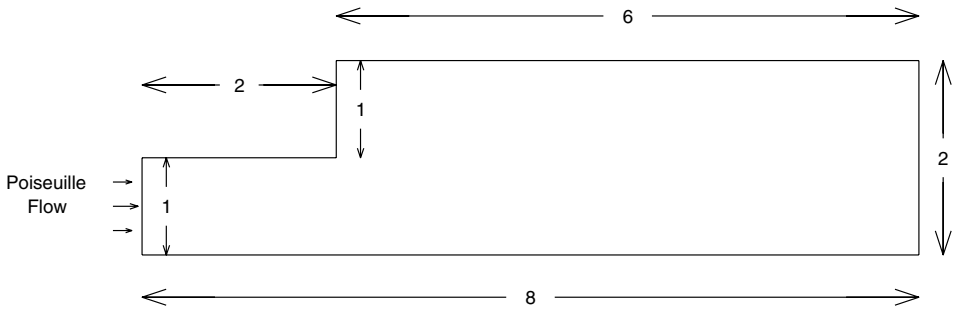

Fig. 2. Backward facing step.

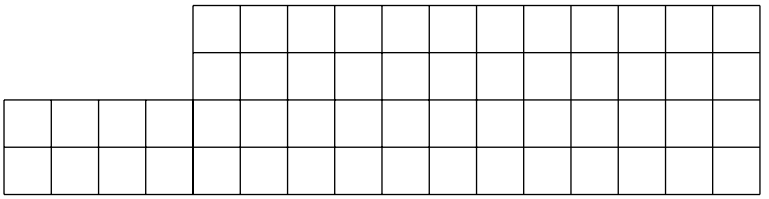

Fig. 3. Planar backward facing step grid at $n_y = 4$.

Table 11
Axial flow in the solution of the S and S_W functionals with enclosed flow conditions

n_y	Axial flow					
	$x = -2$	$x = 0$		$x = 3$		$x = 6$
		S	S_W	S	S_W	
4	0.16667	0.10837	0.16532	0.13574	0.16604	0.16667
8	0.16667	0.13361	0.16611	0.14913	0.16638	0.16667
16	0.16667	0.14942	0.16642	0.15753	0.16654	0.16667
32	0.16667	0.15811	0.16656	0.16214	0.16661	0.16667

Table 12
Axial flow in the solution of the J_h and $J_{h,W}$ functionals

n_y	Axial flow					
	$x = -2$	$x = 0$		$x = 3$		$x = 6$
		J_h	$J_{h,W}$	J_h	$J_{h,W}$	
4	0.16667	0.05786	0.16534	0.10781	0.16604	0.16667
8	0.16667	0.09273	0.16617	0.12724	0.16641	0.16667
16	0.16667	0.12364	0.16647	0.14379	0.16656	0.16667
32	0.16667	0.14443	0.16659	0.15487	0.16662	0.16667

The J_h and $G_{1,h}$ formulations give quite similar results to each other, with considerably less flow lost in the solution of the S formulation; contrast the appropriate columns in Table 11 with those in Tables 12 and 13. All solutions are poor although we acknowledge that the exponents we have applied to the

Table 13
Axial flow in the solution of the $G_{1,h}$ and $G_{1,h,W}$ functionals

n_y	Axial flow					
	$x = -2$	$x = 0$		$x = 3$		$x = 6$
		$G_{1,h}$	$G_{1,h,W}$	$G_{1,h}$	$G_{1,h,W}$	
4	0.16667	0.05694	0.16535	0.10851	0.16605	0.16667
8	0.16667	0.08863	0.16617	0.12532	0.16641	0.16667
16	0.16667	0.11892	0.16646	0.14137	0.16656	0.16667
32	0.16667	0.14122	0.16659	0.15319	0.16662	0.16667

Table 14
Axial flow in the solution of the S and S_W functionals with downstream stress conditions

n_y	Axial flow						
	$x = -2$	$x = 0$		$x = 3$		$x = 6$	
		S	S_W	S	S_W	S	S_W
4	0.16667	0.10255	0.16513	0.09919	0.16526	0.09919	0.16530
8	0.16667	0.12922	0.16602	0.12727	0.16600	0.12727	0.16600
16	0.16667	0.14678	0.16638	0.14577	0.16637	0.14577	0.16637
32	0.16667	0.15670	0.16654	0.15620	0.16653	0.15620	0.16653

mesh-dependent factors may not be optimal for a problem in a non-convex domain; see [20]. All three weighted formulations give approximately the same results; compare the results for the S_W formulation in Table 11 with those for the $J_{h,W}$ and $G_{1,h,W}$ formulations in Tables 12 and 13, respectively. With downstream stress conditions the S formulation gives similar results to those for enclosed flow near the re-entrant corner but fluid loss occurs right to the end of the channel; see Table 14. As a pictorial illustration of the results in Figs. 4 and 5 we plot the stream functions of the S and S_W formulations with enclosed flow conditions for the grid $n_y = 8$, so that there is a grid of 8×4 elements in the inlet section and a grid of 24×8 elements in the outlet section. The stream functions have been recovered by minimising the functional

$$S_s = \|\psi_x - U_3\|_0^2 + \|\psi_y - U_4\|_0^2.$$

These figures are typical since all three formulations give broadly similar results. The diverging contours on entry and the converging contours on exit clearly show that much flow is lost in the middle of the pipe in the unweighted case, whereas the parallel lines on entry and exit in the weighted case indicate the true behaviour of the fluid.

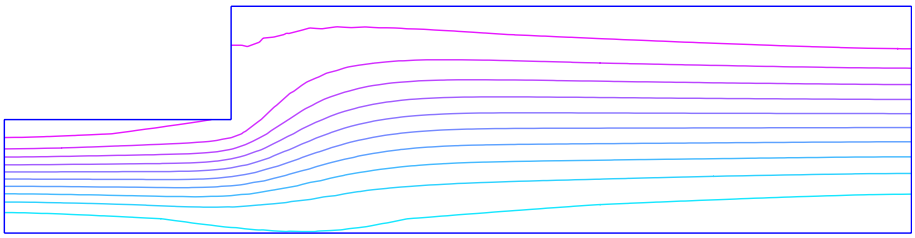

Fig. 4. Stream function in the solution of the S formulation.

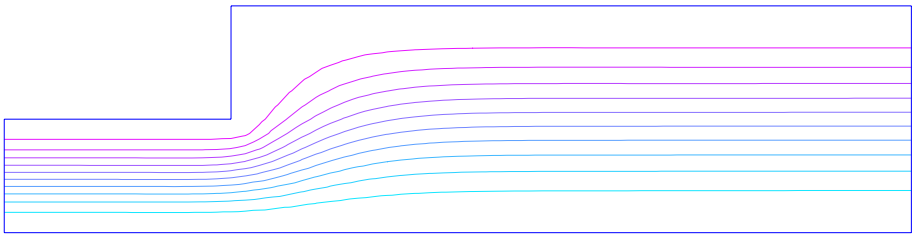

Fig. 5. Stream function in the solution of the S_W formulation.

The solutions of the G_2 and G_3 formulations do not converge at all in this domain, as we would expect from the theory. The velocities in the analytical solution are not in $H^2(\Omega)$ and therefore the components of U as defined by (29) are not in $H^1(\Omega)$.

5. Conclusion

The least-squares finite element method is in principle a very attractive way of simulating incompressible Stokes flow. The linear systems which arise are symmetric and positive-definite; hence fast and simple direct solvers, like banded Choleski, or indirect solvers, like the conjugate gradient method, can be used. Being able to apply the latter in particular can be important in developing an efficient multigrid algorithm.

However, the results we show here make it clear that even for simple flows in convex domains lack of mass conservation can make the approximations extremely inaccurate. All three formulations we have considered share this problem of loss of flow.

Our results show this can be considerably reduced by penalising other terms in the functionals relative to that representing conservation of mass. For this case, the approximations to the velocities in the solutions obtained by minimising the weighted functionals converge at optimal rates in a convex domain.

In the solution of the J formulation, mass may be conserved if certain non-physical conditions are applied; see [8]. We observe a similar phenomenon with the S formulation; see the Appendix.

Appendix A. Boundary conditions for which mass is conserved

We have obtained solutions of the S formulation in the long channel which satisfy the boundary conditions (20). In this case the normal velocity and the tangential stress are specified on the boundary. Results for this case are presented in the following tables.

We see from Table A.1 that no mass is lost when these conditions are specified. Furthermore the velocities converge at order h^2 in L^2 and order h in H^1 between all the grids, even with equal weights on each

Table A.1
Axial flow in the solution of the S functional

$n_x \times n_y$	Axial flow				
	$x = 0$	$x = 5$	$x = 10$	$x = 15$	$x = 20$
80×4	0.15625	0.15625	0.15625	0.15625	0.15625
160×8	0.16406	0.16406	0.16406	0.16406	0.16406
320×16	0.16602	0.16602	0.16602	0.16602	0.16602
640×32	0.16650	0.16650	0.16650	0.16650	0.16650
1280×64	0.16663	0.16663	0.16663	0.16663	0.16663

Table A.2
Errors in the solution of the S functional

$n_x \times n_y$	Errors in the solution of the S functional	
	$\|\vec{u} - \vec{u}_h\|_{0,2}$	$\|\vec{u} - \vec{u}_h\|_{1,2}$
80×4	0.04759	0.59211
160×8	0.01189	0.29593
320×16	0.00297	0.14793
640×32	7.42×10^{-4}	0.07396
1280×64	1.86×10^{-4}	0.03698

equation term; see Table A.2. We have also found that mass is conserved in the solutions when we enforce the boundary conditions (21), the tangential velocity and normal stress; see [10].

It is known that solutions of the planar J formulation display no loss of mass when the pressure together with either $\vec{u} \cdot \hat{n}$ or $\vec{u} \cdot \hat{s}$ are given on the boundary and that furthermore the J functional (25) is equivalent to an H^1 norm when these conditions are applied; see [6,7,8,25].

However none of these conditions are canonical ones for the second-order Stokes system (3) and (4). Additionally they cannot usually be deduced for a given physical problem. Hence their practical uses are very limited.

References

[1] I.O. Arushanian, G.M. Kobelkov, Implementation of a least-squares finite element method for solving the Stokes problem with a parameter, Numer. Linear Algebr. Appl. 6 (1999) 587–597.
[2] A. Aziz, R. Kellog, A. Stephens, Least-squares methods for elliptic systems, Math. Comput. 10 (1985) 53–70.
[3] D.M. Bedivan, Error estimates for least squares finite element methods, Comput. Math. Appl. 43 (2002) 1003–1020.
[4] P. Bochev, Analysis of least-squares finite element methods for the Navier–Stokes equations, SIAM J. Numer. Anal. 34 (1997) 1817–1844.
[5] P. Bochev, Negative norm least-squares methods for the velocity–vorticity–pressure Navier–Stokes equations, Numer. Meth. Part. Diff. Eq. 15 (1999) 237–256.
[6] P. Bochev, M.D. Gunzburger, Accuracy of least-squares methods for the Navier–Stokes equations, Comput. Fluids 22 (1993) 549–563.
[7] P. Bochev, M.D. Gunzburger, Analysis of least-squares methods for the Stokes equations, Math. Comput. 63 (No. 208) (1994) 479–506.
[8] P. Bochev, M.D. Gunzburger, Finite element methods of least squares type, SIAM Rev. 40 (1998) 789–837.
[9] D. Boffi, F. Brezzi, L. Gastaldi, On the problem of spurious eigenvalues in the approximation of linear elliptic problems in mixed form, Math. Comput. 6 (2000) 121–140.
[10] P. Bolton, A least-squares finite element method for the Stokes and Navier–Stokes equations, Ph.D. Thesis, UMIST, 2002.
[11] P. Bolton, J. Stratakis, R.W. Thatcher, Mass conservation in least squares methods for Stokes flow, Manchester Centre for Computational Mathematics Report 376, Manchester University/UMIST, 2001.
[12] Z. Cai, T.A. Manteuffel, S.F. McCormick, First-order system least squares for the Stokes equations, with applications to linear elasticity, SIAM J. Numer. Anal. 34 (1997) 1727–1741.
[13] Z. Cai, T.A. Manteuffel, S.F. McCormick, First-order system least squares for velocity–vorticity–pressure form of the Stokes equations with applications to linear elasticity, ETNA 3 (1995) 150–159.
[14] Z. Cai, X. Ye, A least-squares finite element approximation to the compressible Stokes equations, Numer. Meth. Part. Differential Eq. 16 (2000) 62–70.
[15] C.-L. Chang, An acceleration pressure formulation, Appl. Math. Comput. 36 (1990) 135–146.
[16] C.-L. Chang, M.D. Gunzburger, A finite element method for first order elliptic systems in three dimensions, Appl. Math. Comput. 23 (1987) 171–184.
[17] C.-L. Chang, B.-N. Jiang, An error analysis of least-squares finite element method of velocity–pressure–vorticity formulation for the Stokes problem, Comput. Meth. Appl. Mech. Eng. 84 (1990) 247–255.
[18] C.-L. Chang, J.J. Nelson, Least-squares finite element method for the Stokes problem with zero residual of mass conservation, SIAM J. Numer. Anal. 34 (1997) 480–489.

[19] C.-L. Chang, S.Y. Yang, Analysis of the L^2 least-squares finite element method for the velocity–vorticity–pressure Stokes equations with velocity boundary conditions, Appl. Math. Comput. 130 (2002) 121–144.
[20] J.M. Deang, M.D. Gunzburger, Issues related to least-squares finite element methods for the Stokes equations, SIAM J. Sci. Comput. 20 (1998) 878–906.
[21] F. Dubois, Vorticity–velocity–pressure formulation for the Stokes problem, Math. Meth. Appl. Sci. 25 (2002) 1091–1119.
[22] J.M. Fiard, T.A. Manteuffel, S.F. McCormick, First-order system least squares (FOSLS) for convection–diffusion problems: numerical results, SIAM J. Sci. Comput. 19 (1998) 1958–1979.
[23] G.J. Fix, M.D. Gunzburger, R.A. Nicolaides, On finite element methods of the least squares type, Comput. Math. Appl. 5 (1979) 87–98.
[24] G.J. Fix, M.D. Gunzburger, R.A. Nicolaides, On mixed finite element methods for first order elliptic systems, Numer. Math. 37 (1981) 29–48.
[25] B.-N. Jiang, The Least-Squares Finite Element Method, Theory and Applications in Computational Fluid Dynamics and Electromagnetics, Scientific Computation Series, Springer, New York, 1998.
[26] B.-N. Jiang, G.F. Carey, Adaptive refinement for least-squares finite elements with element-by-element conjugate gradient solution, Int. J. Numer. Meth. Eng. 24 (1987) 569–580.
[27] B.-N. Jiang, C.-L. Chang, Least-squares finite elements for the Stokes problem, Comput. Meth. Appl. Mech. Eng. 78 (1990) 297–311.
[28] B.-N. Jiang, L.A. Povinelli, Least-squares finite element method for fluid dynamics, Comput. Meth. Appl. Mech. Eng. 81 (1990) 13–37.
[29] P. Lynn, S. Arya, Use of least-squares criterion in the finite element method, Int. J. Numer. Meth. Eng. 6 (1973) 75–88.
[30] D.J. Silvester, R.W. Thatcher, The effect of stability of mixed finite element approximations on the accuracy and rate of convergence of solutions, Int. J. Numer. Meth. Fluids 6 (1986) 841–853.
[31] R.W. Thatcher, A least squares method for Stokes flow based on stress and stream functions, Manchester Centre for Computational Mathematics Report 330, Manchester University/UMIST, 1998.
[32] R.W. Thatcher, A least squares method for biharmonic problems, SIAM J. Numer. Anal. 38 (2000) 1523–1539.
[33] W.L. Wendland, Elliptic Systems in the Plane, Pitman, London, 1979.
[34] X. Ye, Domain decomposition for least-squares finite element methods for the Stokes equations, Appl. Math. Comput. 97 (1998) 45–53.